一般社団法人　電子情報通信学会
THE INSTITUTE OF ELECTRONICS,
INFORMATION AND COMMUNICATION ENGINEERS

信学技報
IEICE Technical Report
A・P2020-57(2020-09)

Wideband Transmitarray Antennas Design Using 1-Bit Polarization-Rotation Elements

Sen LIU† Qiang CHEN†

† Department of Communications Engineering, Tohoku University Aoba-6-6-5 Aramaki, Aoba-ku, Sendai, 980-0845 Japan

E-mail: † liu.sen.s3@dc.tohoku.ac.jp, chenq@ecei.tohoku.ac.jp

Abstract Three different 1-bit phase-quantization transmitarray elements exploiting polarization-rotation technique are presented in this paper for wideband transmitarray antennas. The elements demonstrate extremely wide 1-dB bandwidth. Besides, the full transmitarray system design process can be greatly simplified by introducing 1-bit phase quantization technique. Phase matching optimization is performed to determine the pattern distribution on the transmitarray apertures for all cases. The full-wave simulations have been carried out to verify the designs. Reasonable consistent radiation patterns are obtained for each case, which directly reveals the wideband feature of the developed transmitarray antennas. Specifically, the 1-dB fractional realized gain bandwidth of 31%, 25%, and 52% are achieved, respectively.

Keywords Antenna arrays, Periodic structures, Polarization rotation, Transmitarrays, Wideband

1. INTRODUCTION

Transmitarray antennas (TAs), as a potential alternative to phased arrays and lens antennas, have drawn increasing attention in recent years. They typically convert the spherical wave front radiated from the source feed to planar wave front, forming a pencil beam in desired direction. Although TAs can provide advantages of low profile, easy-of-fabrication, low cost, and versatile radiation performance, they suffer from inherent narrow bandwidth due to bandwidth limitation of elements and differential spatial phase delay [1]. Many research works have been reported to overcome this limitation, e.g., true-time-delay configurations [2], and phase matching optimization [3].

Phase discretization is a technique that has been widely deployed in reconfigurable transmitarrays [4] due to its simplicity and reduced complexity and cost. Typical 1-bit phase quantization discretizes full 360° phase into two individual states with phase difference of 180° between them.

In this paper, inspired by the polarization-rotation technique in [5], together with 1-bit phase quantization, three 3-layer transmitarray elements are developed to design wideband TAs. On one hand, due to multiple reflection and transmission occurring inside the unit cells, the transmissive polarization-rotation efficiency is very high. Besides, wideband performance can be obtained by properly designing the structures in the middle layer. On the other hand, the entire design process can be greatly simplified by exploiting 1-bit phase quantization technique to compensate spatial phase delay. Moreover, phase matching optimization is performed to minimize the weighted overall phase error. The design concept has been validated in full-wave simulations. All three configurations can provide reasonable wideband performance with simple design process, revealing great potential in wideband reconfigurable design.

2. WIDEBAND TAS DESIGN

Based on polarization-rotation technique, three wideband TA unit-cells are developed. The 3-D topological structure is shown in Fig. 1(a). The physical dimensions are $15\,\text{mm} \times 15\,\text{mm}$, which are equivalent to $0.5\lambda_0 \times 0.5\lambda_0$, where λ_0 is the free-space wavelength at 10 GHz. It consists of three layers. The top and bottom layers are two metallic orthogonal grid polarizers with a width of $w = 0.8\,\text{mm}$ and a gap of $s = 2.2\,\text{mm}$, which work as lens or reflector depending on the metal wire grids orientation. A $d = 4\,\text{mm}$ air gap is inserted between each layer. Besides, all the metallic structures are printed on a $t = 0.8\,\text{mm}$ thick substrate with relative dielectric constant of 3.3 and loss tangent of 0.001. The three unit-cells have identical structures except for the middle layers, which are shown in Fig. 1 (b)-(d), respectively. 1-bit phase quantization is formed simply by mirroring the middle layers for all cases to compensate spatial phase delay.

The unit cell performance under normal incidence is simulated using infinite structure approximation with periodic boundary conditions. The performance of T_{xy} (the first letter of the subscript denotes the polarization of the transmitted fields, along with the second letter for that

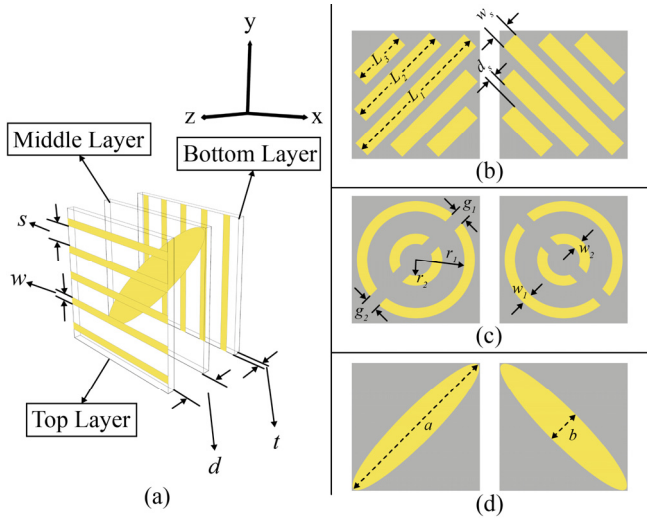

Fig. 1 (a) 3-D topological structure; (b) middle layer of the stripline unit; (c) middle of layer of the split ring unit; (d) middle layer of the ellipse unit. $w = 0.8$, $s = 2.2$, $d = 4.0$, $t = 0.8$, $L_1 = 18.0$, $L_2 = 12.5$, $L_3 = 6.5$, $w_s = 2.0$, $d_s = 1.0$, $r_1 = 5.7$, $g_1 = 1.5$, $w_1 = 1.2$, $r_2 = 1.9$, $g_2 = 1.5$, $w_2 = 1.2$, $a = 10.3$, $b = 2$ in mm.

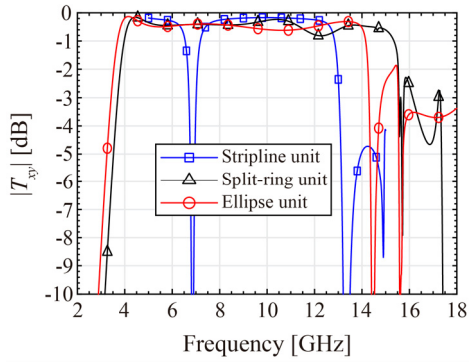

Fig. 2 Magnitude responses of T_{xy} for all unit-cells.

of the incident fields) is of critical concern, as it represents the real physical polarization-rotation process. Fig. 2 shows the magnitude responses. Fig. 3 shows the phase responses. Obviously, polarization-rotation with high purity can be obtained within wide frequency band for all three elements. Specifically, these unit-cells provide -1-dB bandwidth from 7.2-12.8 GHz, 4.0-15.3GHz, and 3.7-14.2 GHz, respectively. Moreover, the phase difference of 180° can be observed over the entire operation band.

A wideband low-profile printed antipodal fermi tapered slot antenna (APFA) [6] is employed to efficiently illuminate the TA apertures. Fig. 4 show the simulated reflection coefficient with the inset of the schematic view of the APFA. The bandwidth is defined as $|S_{11}| < -10$ dB covering the band of 5.5-14.5 GHz, which is adequate for the three unit-cells.

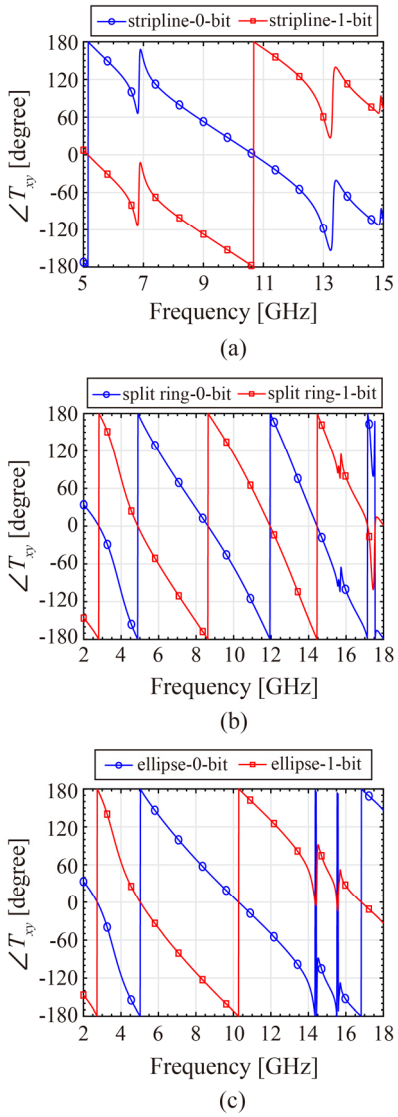

Fig. 3 Phase responses of T_{xy} for (a) stripline unit; (b) split ring unit; (c) ellipse unit.

The TA apertures is configured to rectangle to match with the asymmetric radiation patterns of the APFA. The schematic of the model is shown in Fig. 5, where L, D, and H represent the length of the aperture, the width of the aperture, and the feeding distance, respectively. Besides, phase matching optimization is performed to determine the pattern distribution of the middle layer for each case. The cost function of the optimization loop is described as:

$$COST = \sum_{f} a(f) \times \left(\sum_{mn} A_{mn}(f) \cdot \left| \psi_{mn}^{achieve}(f) - [-\psi_{mn}^{inc}(f) + c(f)] \right| \right) \quad (1)$$

where $a(f)$ denotes the weight at each frequency point,

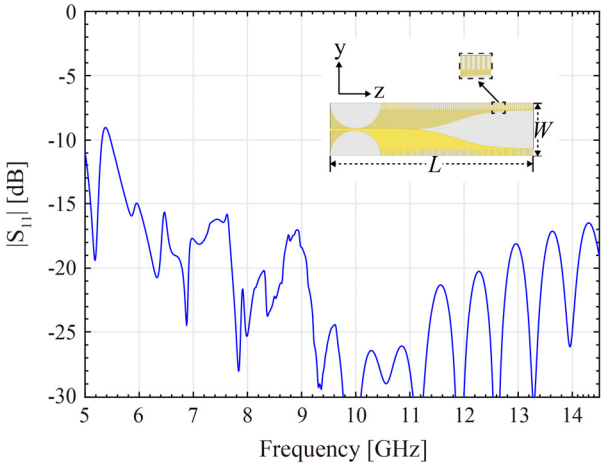

Fig. 4 Reflection coefficient response of the APFA. Inset: schematic of the APFA. $L = 160$, $W = 42$ in mm.

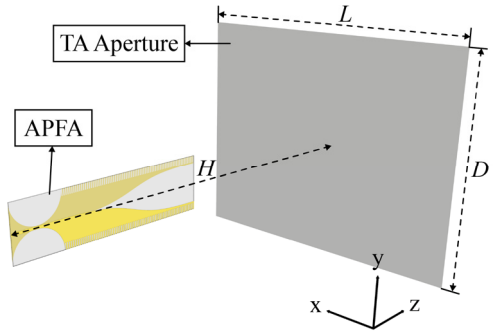

Fig. 5 TA system model. $H = 330$, $L = 285$, $D = 225$ in mm.

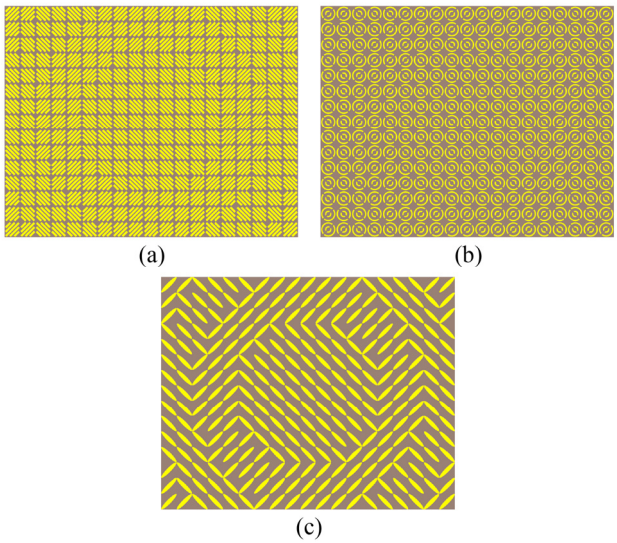

Fig. 6 Pattern distribution of the middle layer for (a) stripline unit; (b) split ring unit; (c) ellipse unit.

$A_{mn}(f)$ represents the magnitude distribution of the incident field on the aperture at certain frequency point, $\Psi_{mn}^{achieve}(f)$ is the achievable compensation phase value at certain frequency point, $\Psi_{mn}^{inc}(f)$ is the incident phase value at certain frequency point, and $c(f)$ is the constant reference phase for each frequency point. The purpose of the optimization is to minimize the overall phase error to balance the bandwidth performance and aperture efficiency. Meanwhile, due to the simplicity of the calculation and the high efficiency of the optimization loop, the entire optimization process is very time-efficient. The optimal pattern distributions are shown in Fig. 6 for each case.

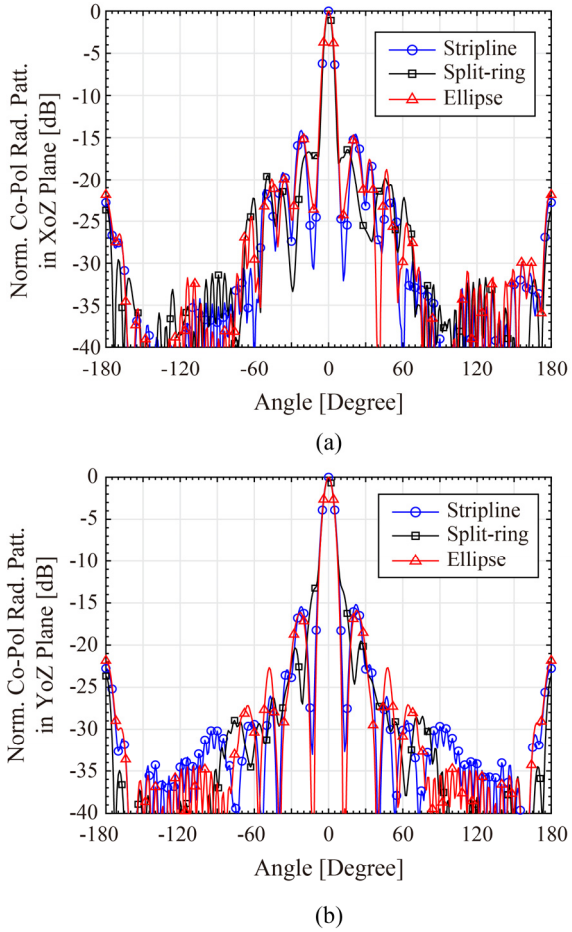

Fig. 7 Normalized Co-Pol radiation patterns at 10 GHz in (a) XoZ plane; (b) YoZ plane.

Full-wave simulations are performed to validate the design. Fig. 7 shows the simulated normalized Co-Pol radiation patterns at 10 GHz for all cases. The simulated results show consistency between each case in main beam region. Besides, 3-dB beamwidth responses are presented in Fig. 8, which indicate radiation consistency for all cases. It should be noticed that, due to rectangular shape of the apertures, the beamwidth in XoZ plane is reasonably narrower than that in YoZ plane. Fig. 9 shows the simulated realized gain responses for all cases. The 1-dB gain bandwidth is defined from its value at 10 GHz,

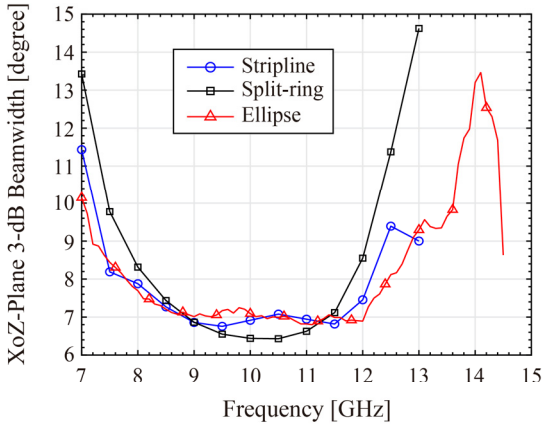

(a)

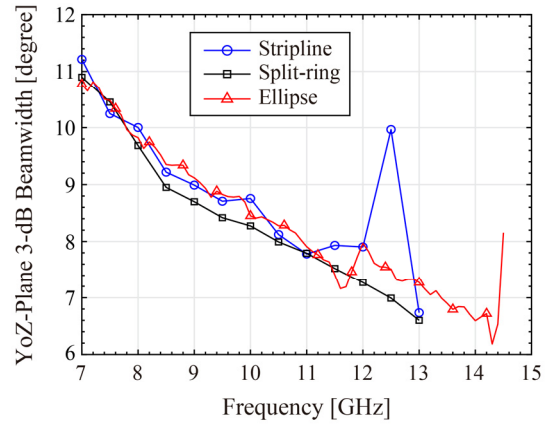

(b)

Fig. 8 3-dB beamwidth responses in (a) XoZ plane; (b) YoZ plane.

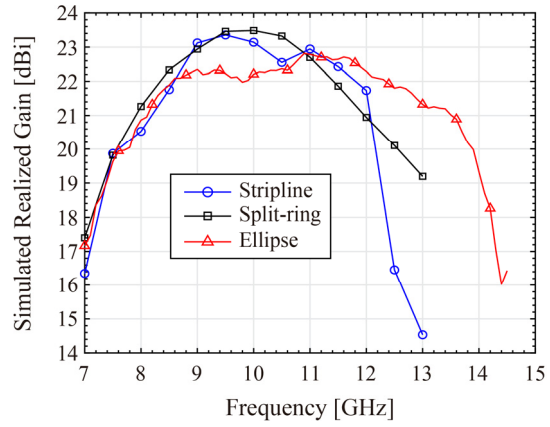

Fig. 9 Simulated realized gain responses.

corresponding to 8.6-11.7 GHz, 8.6-11.1 GHz, and 8.2-13.4 GHz for stripline case, split ring case, and ellipse case, respectively. The 1-dB fractional bandwidth is 31%, 25%, and 52%, respectively. It should be mentioned that the bandwidths of TAs are still much lower than those of the unit cells. The reason is the differential spatial phase delay resulting from the different lengths from the source feed to each element on the TA aperture makes it inevitable that elements suffer from large phase errors over wide frequency range. Therefore, a source feed that can match the phase conditions is crucial to further expand the bandwidth limitation for such TAs.

3. Conclusion

Three different 1-bit phase-quantization elements utilizing polarization-rotation technique have been presented in this paper for wideband TAs. Besides, phase matching optimization has been performed to determine the pattern distribution for each case. The simulated results show reasonable wideband performance for each configuration. The physical limitation of such configurations has also been analyzed. In addition to their wideband feature, the simplicity of their design makes them suitable for developing wideband reconfigurable TAs.

Acknowledgement

This research was supported by Program on Open Innovation Platform with Enterprises, Research Institute and Academia, Japan Science and Technology Agency (JST, OPERA, JPMJOP1852).

References

[1] A. H. Abdelrahman, F. Yang, A. Z. Elsherbeni, and P. Nayeri, *Analysis and Design of Transmitarray Antennas*. San Francisco, CA, USA: Morgan & Claypool, 2017.

[2] M. Li, M. A. Al-Joumayly, and N. Behdad, "Broadband True-Time-Delay Microwave Lenses Based on Miniaturized Element Frequency Selective Surfaces," *IEEE Trans. Antennas Propag.*, vol. 61, no. 3, pp. 1166-1179, Mar. 2013.

[3] A. H. Abdelrahman, P. Nayeri, A. Z. Elsherbeni, and F. Yang, "Bandwidth Improvement Methods of Transmitarray Antennas," *IEEE Trans. Antennas Propag.*, vol. 63, no. 7, pp. 2946-2954, Jul. 2015.

[4] A. Clemente, L. Dussopt, R. Sauleau, P. Potier, and P. Pouliguen, "Wideband 400-Element Electronically Reconfigurable Transmitarray in X Band," *IEEE Trans. Antennas Propag.*, vol. 61, no. 10, pp. 5017-5027, Oct. 2013.

[5] N. K. Grady, J. E. Heyes, D. R. Chowdhury, Y. Zeng, M. T. Reiten, A. K. Azad, A. J. Taylor, D. A. R. Dalvit, and H.-T. Chen, "Terahertz Metamaterials for Linear Polarization Conversion and Anomalous Refraction," *Science*, vol. 340, no. 6138, pp. 1304, Jun. 2013.

[6] M. Sato, H. Sato, T. Hirose, H. Kobayashi, K. Sawaya, and K. Mizuno, "Antipodal LTSA with Corrugation for 94-GHz band Passive Millimeter-wave Imager," in *Proceedings of Asia-Pacific Microwave Conference 2007*, 2007, pp. 1-4.